DOI: https://doi.org/10.1016/j.apcatb.2017.06.004

Thermocatalytic conversion of lignin in an ethanol/formic acid medium with NiMo catalysts: role of the metal and acid sites

Mikel Oregui-Bengoechea[a], Nemanja Miletić[b], Sveinung F. Simonsen[a], Audun Kronstad[a], Inaki Gandarias[b], Pedro L. Arias[b] and Tanja Barth[a]

[a] *Department of Chemistry, University of Bergen, Norway, Allegaten 41, N-5007 Bergen, Norway*

[b] *Department of Chemical and Environmental Engineering, School of Engineering, University of the Basque Country (EHU/UPV), C/Alameda Urquijo s/n,48013 Bilbao, Spain*

Keywords: lignin, formic acid, NiMo catalyst, alumina, zirconia

Abstract

NiMo catalysts supported on different sulfated and non-sulfated aluminas and zirconias were studied for the catalytic conversion of lignin in a formic acid/ethanol medium. All the pre-reduced NiMo-support combinations resulted in high conversion of lignin into bio-oil, with over 60 % yield (mass %). The NiMo-sulfated alumina catalyst exhibited the highest activity among all the catalyst studied. The overall reaction mechanism of the catalytic lignin conversion was found to be especially complex. The oil yield and its properties are affected by a combination of successive catalytic reactions that are part of the lignin conversion process. Lignin is first de-polymerized into smaller fragments through the cleavage of the aliphatic ether bonds. This reaction can be either catalyzed by Ni^0 species and strong Lewis acid sites within the alumina supports. In the presence of both active species, the Ni^0 catalyzed ether bond cleavage is the prevailing reaction mechanism. In a second step, the smaller lignin fragments can be stabilized by catalytic hydrodeoxygenation (HDO) and alkylation reactions that hinder their re-polymerization into char. Mo was found to be especially active for HDO reactions while all the catalyst studied exhibited significant alkylation activity. The final bio-oil yield is strongly dependent on the aliphatic ether bond cleavage rate; the contribution of those monomer stabilization reactions (i.e. HDO and alkylation) being secondary.

1. Introduction

The use of lignocellulosic biomass as a raw material for the production of renewable fuels and chemicals is growing rapidly. Consequently, there is an increasing interest in the development of integrated models for the efficient valorization of woody biomass (i.e. as lignocellulosic bio-refineries). Over the last decades, most of the effort has been focused on the development of more efficient lignocellulose pretreatment technologies and the subsequent conversion of the cellulose and hemicellulose fraction into bio-ethanol [1-3] and/or value-added chemicals [4]. In contrast, the third component, lignin, is mostly considered a waste and it is normally burned as a low value fuel [5]. However, the expected growth of the production of lignocellulosic-based products will demand the efficient valorization of the lignin sub-product and the conceptual integration of its conversion processes in the so-called bio-refinery concept.

A plausible process that could meet these requirements is the recently developed LtL process [6, 7]. Formic acid, one of the main sub-products from the cellulose and hemicellulose

hydrolysis and sugar conversion processes [8, 9], can react together with lignin in an ethanol media to yield a mono-aromatic based oil, with considerable chemical stability and low oxygen content. This process is carried out under severe reduction conditions: formic acid is decomposed mainly into CO_2 and H_2 providing high reaction pressures. Nevertheless, the LtL conversion requires high temperatures, in the range of 300-360 °C, and long residence times for complete lignin conversion. The process severity would imply a high cost at industrial scale, and at present, the oil yields and its quality are not sufficient to produce LtL oils competitive with traditional fossil-based products [10, 11].

A possible option in order to decrease the process severity and simultaneously increase the LtL oil yield and quality – i.e. a higher H/C and lower O/C ratio- is the use of heterogeneous catalysts. Recently Zhang and co-workers [12] described the most important catalytic routes for the conversion of lignin in a reductive environment (hydroprocessing), and the most relevant conversion mechanism were: (i) the catalytic hydrogenolysis of the aliphatic ether bonds of the lignin biopolymer and (ii) the catalytic hydrodeoxygenation (HDO) of the lignin monomers. For the catalytic hydrogenolysis of lignin, Ni-based catalysts are normally the preferred choice (e.g., Raney Ni, Ni/SiO_2, Ni/activated carbon) [13-15]. In the case of HDO, nonetheless, three different types of catalysts have been studied: monometallic, bimetallic and bifunctional. The monometallic catalysts consist mainly of Mo-supported catalysts [12]. The bimetallic systems refer typically to the combination of mixed sulfides of Co, Ni, Mo and W. Nevertheless, sulfided catalysts are not entirely adequate since they increase the amount of sulfur containing compounds in the liquid products [12, 16]. Bifunctional catalysts in turn contain both metal and acid sites [17]. Several combinations of hydrogenating (e.g. Ni Raney, Pd/C, Pt/Al_2O_3) and solid-acid catalysts (e.g. HZSM-5 and Nafion/SiO_2) [18-20], or even bifunctional catalysts (e.g. Ru/HZSM-5, Ni/HZSM-5) [21, 22] have been studied, mostly with lignin model compounds as starting materials.

However, very little research has been conducted in the catalytic hydroprocessing of a real lignin feedstock [12, 23]; and even less in the formic acid aided lignin conversion [24]. In a previous study, we investigated the role of formic acid and the solvent (i.e. ethanol) in the catalytic lignin conversion with a NiMo supported on a sulfated Al_2O_3, a Lewis solid acid [25]. The investigations revealed that the catalytic lignin conversion into bio-oil follows a complex reaction pathway. In the presence of formic acid, lignin undergoes de-polymerization through a

formylation-deformylation-hydrogenolysis pathway that leads to the cleavage of its aliphatic ether bonds. The depolymerized monomers and oligomers can undergo subsequent hydrodeoxygenation (HDO) and alkylation reactions. These reactions tend to stabilize the lignin monomers hindering their re-polymerization into char (Scheme 1).

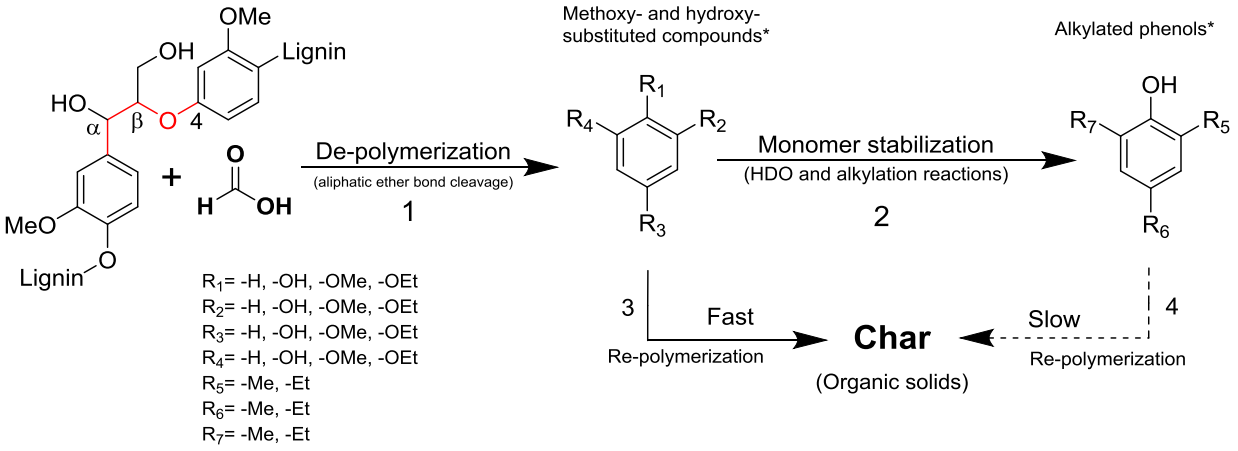

Scheme 1. Sequential reaction scheme for the conversion of lignin into bio-oil. * The term compounds may refer to both monomers and/or oligomers. This is an adapted scheme based on a previous study [25].

To further explore these processes, the catalytic role of the type of metal (i.e. Ni and Mo), the Lewis acidity and the metal-support interaction on the lignin de-polymerization (i.e. aliphatic ether bond cleavage) and monomer stabilization reactions (i.e. HDO and alkylation) is studied using well-characterized heterogeneous catalysts. Moreover, the relative importance of each reaction pathway (de-polymerization vs. stabilization) on the oil yield and oil quality is also assessed. For this purpose, several combinations of non-sulfided monometallic (*i.e.* Ni and Mo) and bimetallic NiMo catalysts supported on zirconia and γ-alumina are evaluated. Sulfated zirconia [26, 27] and alumina [28] are also used as catalyst supports to further explore the effect of the Lewis acidity strength in the reaction mechanism. The recyclability of the NiMo catalyst in the LtL conversion process is also examined.

2. Experimental

2.1 Chemicals

Formic acid (>98%), tetrahydrofuran (>99.9%), ethyl acetate (99.8%), hexadecane (>99.8%), sulfuric acid (95-97%), anhydrous sodium sulphate (>99.0 %) and zirconium (IV) hydroxide (97%) were purchased from Sigma Aldrich and used as supplied. γ-alumina (>97%), nickel(II) nitrate hexahydrate (99.9+% Ni) and ammonium molybdate tetrahydrate (99.98% Mo) were purchased from Strem Chemicals Inc and used as received. The Technical College of Bergen supplied rice straw lignin from a strong acid carbohydrate dissolution pre-treatment. The lignin was ground and sieved (<500 μm) prior to use. The elemental composition and the inorganic ash content of the rice straw lignin are given in Table S1, *Supplementary Information*.

2.2 Synthesis of the catalyst

2.2.1 Synthesis of the supports

Non-sulfated alumina: γ-alumina was dried at 100 °C for 24 h prior to use. This support is named AL.

Non sulfated zirconia: ZrO_2 was obtained by calcining $Zr(OH)_4$ at 600 °C for 4 h with a heating ramp of 3°C/min. The resulting support is denoted as ZR.

Sulfated alumina: γ-alumina was subjected to a thermal treatment in air at 450 °C for 4 h with a heating ramp of 3 °C/min. The calcined alumina was impregnated (4 cm^3 sulfuric acid/cm^3 of pore) with a sulfuric acid solution (mass fraction of 0.5 %) and stirred for 24 hours. The solution was dried at 80 °C for 24 h and the resulting solid was calcined at 600 °C for 4 h with a heating ramp of 3 °C/min. The resulting sulfated alumina is denoted as SAL.

Sulfated zirconia: $Zr(OH)_4$ was impregnated (5 mL/g) with a sulfuric acid solution (0.5 M) and stirred for 2 h. The solution was dried at 80 °C for 24 h and the resulting solid was calcined at 600 °C for 4 h with a heating ramp of 3 °C/min, obtaining the sulfated zirconia (SZ). This support is denoted as S-ZR.

2.2.2 Synthesis of the metallic catalysts

The bimetallic catalysts were later prepared by successive incipient-wetness impregnation of the corresponding support (AL, SAL, ZR and SZR) with an aqueous solution of ammonium molybdate ($(NH_4)_6Mo_7O_{24}\cdot 4H_2O$) and/or nickel nitrate ($Ni(NO_3)_2\cdot 6H_2O$). The nominal loading of MoO_3 and NiO are 12 % and 5 % respectively, given as mass fraction percentage. After impregnation, the catalysts were dried at 105 °C for 20 min and calcined in an air flow (10 mL/min) at 570 °C for 2 h with a heating ramp of 2 °C/min. Later, the solids were subjected to pre-reduction (activation) under a hydrogen flow (10% v/v) at 550 °C for 2 h with a heating ramp of 2 °C/min and used shortly after the treatment. The resulting bimetallic catalysts are named H-NiMo-AL, H-NiMo-SAL, H-NiMo-ZR and H-NiMo-SZR. Two monometallic catalysts were synthesized with the SAL support: one containing only Ni (H-Ni-SAL) and the second containing only Mo (H-Mo-SAL). The metal loading and the synthesis procedure were equivalent to the ones used for their bimetallic counterparts.

The bare supports (AL, SAL, ZR and SZR) were analyzed by N_2-adsorption, FT-IR of adsorbed pyridine, NH_3-TPD, and XRD. The bimetallic H-NiMo-AL, H-NiMo-SAL, H-NiMo-ZR, H-NiMo-SZR, H-Ni-SAL and H-Mo-SAL catalysts were analyzed by N_2-adsorption, NH_3-TPD, ICP-EAS, XRD, TPR and CO-chemisorption. The experimental procedures for the characterization of the catalyst are described in the *Supplementary Information*.

2.3 LtL experiments

2.3.1 Experimental set-up

A detailed description is given elsewhere by Oregui Bengoechea *et al.*[10]. Briefly summarized, lignin (2.0 g), formic acid (1.5 g), ethanol (2.5 g) and the catalyst (0.2 g) were added to a stainless steel reactor (Parr 4742 non-stirred reactor, 25 mL volume). The reactor was closed and heated up to 340 °C in a Carbolite LHT for 6 h. Two replicates were performed for each experiment. The results refer to the average values of both experiments. The amounts of the reactants used for all the experiments are summarized in Table S2, *Supplementary Information*.

2.3.2 Work-up procedure

After heating for the predetermined duration, the reactor was cooled down to ambient temperature by natural convection. The liquid mixture within the reactor was extracted with a solution of ethyl acetate:tetrahydrofuran (90:10) and the solid phase (unreacted lignin, reaction products and catalyst) was filtered off. The resulting liquid phase was dried over Na_2SO_4 and concentrated at reduced pressure (160 mm bar) at 40 °C to yield a dark-brown to black liquid. The oil and solid yield are given as mass fraction % and were determined using the following equation:

Oil/Solid Yield (mass fraction %) = dry mass of oil or solids (g)/dry mass of input lignin (g)

For the catalyzed experiments, the solid yield was calculated after subtracting the amount of catalyst introduced. Therefore, the solid yield refers only to the organic solids (char) and the inorganic lignin ashes.

The oil was analyzed by GC-MS and GPC-SEC. Its elemental composition was also determined. The procedures used for the characterization of the oils are described in the Supplementary Information.

2.3.3 Recycling experiments

After the reaction, the solids (organic ashes, inorganic ashes and catalysts) were recovered and calcined at 570 °C for 2h with a heating ramp of 2 °C/min to eliminate the organic residues. The resulting solids (catalyst and inorganic ashes) were pre-reduced at the same conditions described in *Section 2.2.2* and re-used in the LtL process. After the first recycling cycle, a higher amount of solid was recovered due to inorganic ash accumulation in the system. Therefore, to guarantee the proper reduction of the catalyst, in the second recycling cycle the pre-reduction of the catalyst was carried out for 3 h.

Blank experiments were also carried out to evaluate the activity of the inorganic ashes. The experimental procedure is analogous to the one described in *Section 2.3.1*, but in this case, instead of catalysts, 0.2 g of inorganic ashes were added (ASH-1 experiment). The method used to obtain the inorganic lignin ashes is the same used to determine the lignin ash content (*Supplementary Information).*

3. Results

3.1 Catalyst Characterization

3.1.1 N_2-adsorption

The textural properties of the catalysts are presented in Table 1 and Fig. 1. The results show that the sulfating process has different effects on the textural properties of the alumina and zirconia supports. In the case of the alumina catalysts, small differences between the sulfated and non-sulfated counterparts are observed: the sulfated solids display slightly higher surface areas. The alumina-based solids (AL, SAL, H-NiMo-AL and H-NiMo-SAL) exhibit an IUPAC Type IV isotherm typical for mesoporous materials. The catalysts (H-NiMo-AL and H-NiMo-SAL) present a lower surface area and V_t than their corresponding bare supports (AL and SAL) suggesting that the incorporation of the Ni and Mo causes the partial blockage of the pores [29].

Table 1: BET surface area (S_{BET}), total pore volume (V_t), total acidity measurements (NH_3-TPD), NiO and MoO_3 content (ICP-EAS) and number of nickel active sites (CO-chemisorption) for the bare supports (AL, SAL, ZR, SZR) and metallic catalyst (H-NiMo-AL, H-NiMo-SAL, H-NiMo-ZR, H-NiMo-SZR, H-Ni-SAL, H-Mo-SAL).

Entry	Catalyst[a]	S_{BET} (m^2/g)	V_t (cm^3/g)	Acidity (mmol NH_3/g cat.)		ICP-MS		No. of Ni active sites (µmol CO/g cat)
				Weak	Strong	NiO	MoO_3	
				85-340°C	340-590°C	(mass fraction %)		
1	**AL**	198	0.416	0.420	0.390	-	-	-
2	**H-NiMo-AL**	172	0.328	0.521	0.366	4.7	11.4	18.5
3	**SAL**	202	0.414	0.485	0.397	-	-	-
4	**H-NiMo-SAL**	179	0.335	0.547	0.375	3.6	10.7	6.9
5	**H-Ni-SAL**	183	0.369	0.374	0.589	5.8	-	12.6
6	**H-Mo-SAL**	181	0.347	0.467	0.335	-	11.7	-
7	**ZR**	11	0.032	0.056	0.054	-	-	-
8	**H-NiMo-ZR**	15	0.010	0.045	0.026	5.2	11.7	2.1
9	**SZR**	71.2	0.074	0.289	0.126	-	-	-
10	**H-NiMo-SZR**	42.4	0.066	0.146	0.067	4.6	10.0	0.7

[a] **H** refers to those catalyst that were submitted to a pre-reduction treatment, **NiMo:** bimetallic catalysts containing Ni and Mo, **Ni:** monometallic catalyst containing only Ni, **Mo:** monometallic catalyst containing only Mo, **AL:** γ-alumina, **SAL:** sulfated alumina, **ZR:** zirconia and **SZR:** sulfated zirconia

198 The textural properties of the zirconia support, however, are considerably altered upon
199 sulfating. The non-sulfated zirconia solids (ZR and H-NiMo-ZR) exhibit adsorption-desorption
200 isotherms with a hysteresis loop at high relative pressures (Figure 1c) generally assigned to the
201 presence of mesopores [30]. Nevertheless, the low surface area and V_t found in these solids
202 (*entries 7-8*, Table 1) suggest that this hysteresis is due to nanoparticle-aggregation [31]. Thus,
203 the ZR and H-NiMo-ZR solids are either macro- or non-porous. The sulfated zirconia solids
204 (SZR and H-NiMo-SZR), on the other hand, are mesoporous solids and exhibit considerably
205 higher surface areas than their non-sulfated counterparts. The sulfated zirconia solids (SZR and
206 H-NiMo-SZR) show a IUPAC Type IV isotherms (Figure 1d) with a large increase in the
207 adsorption at higher relative pressures (p/p_0), which can be assigned to the presence of large size
208 mesopores in the samples [32]. The isotherms also exhibit a sharp-step H2-type hysteresis loop,
209 which can be explained by the interconnectivity of pores [33, 34]. The SZR support exhibits
210 considerably higher surface area and V_t in comparison to the H-NiMo-SZR catalyst, suggesting
211 that the pores are partially blocked by the Ni and Mo species.

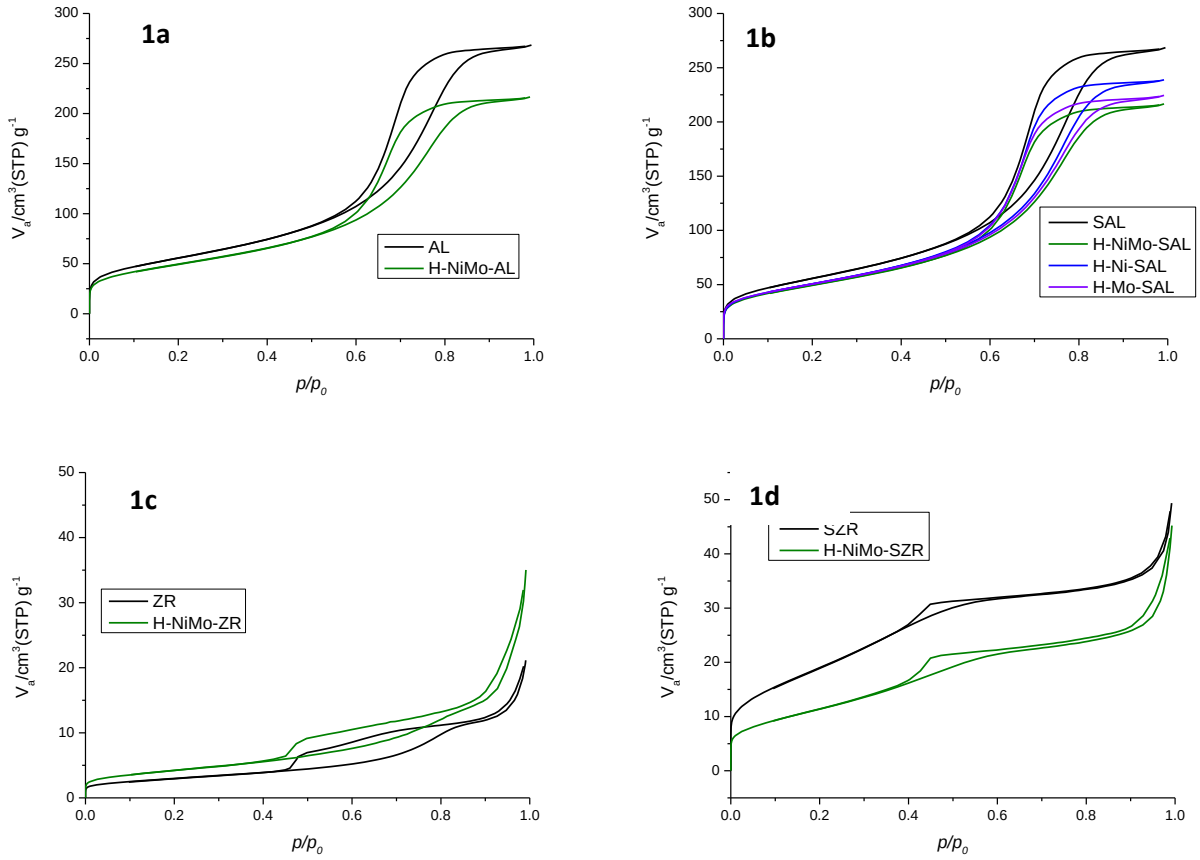

212

213

214 **Figure.1 a)** N_2-adsorption isotherms for the AL (●) and H-NiMo-AL (●) catalysts **b)** N_2-adsorption
215 isotherms for the SAL (●), H-NiMo-SAL (●), H-Ni-SAL (●) and H-Mo-SAL (●) catalysts **c)** N_2-
216 adsorption isotherms for the ZR and H-NiMo-ZR (●) catalysts **d)** N_2-adsorption isotherms for the SZR (●)
217 and H-NiMo-SZR (●) catalysts

218 **3.1.2 Acidity measurements (NH_3-TPD and DRIFT of absorbed pyridine)**

219 NH_3-TPD and DRIFT of absorbed pyridine are normally combined to determine the strength,
220 concentration and type of acid sites (Lewis or Brønsted) within a solid. The NH_3-TPD results are
221 presented in Figure 2 and Table 1, while the DRIFT results are depicted in Figure S1
222 (*Supplementary Information*). In order to facilitate the analysis, the acid sites are further
223 classified according to their strength. This classification is based on NH_3 desorption
224 temperatures. Hence, those acid sites that are not stable below the reaction temperature (<340
225 °C) were designated as weak, while those acid sites that are stable above the reaction temperature
226 (>340 °C) are designated as strong (Table 1).

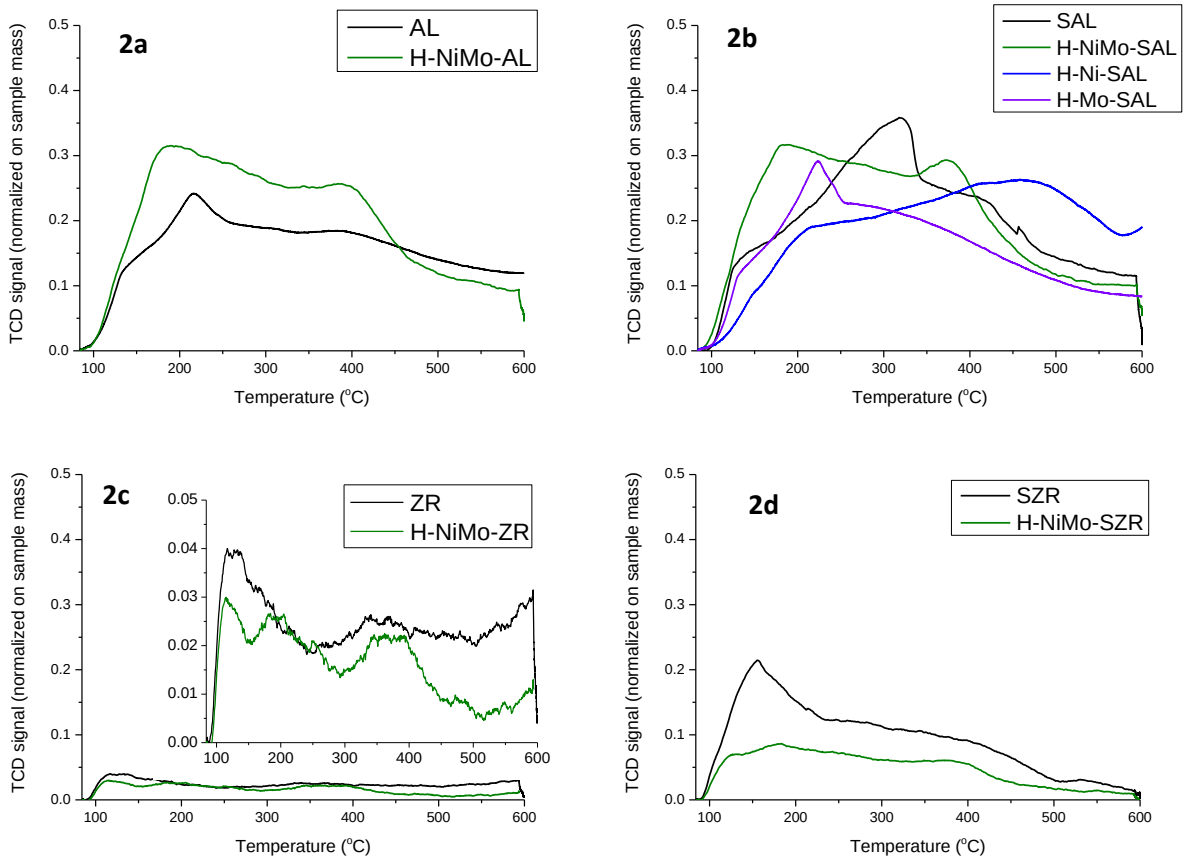

Figure 2a) NH_3-TPD for the AL (●) and H-NiMo-AL (●) catalysts **b)** NH_3-TPD for the SAL (●), H-NiMo-SAL (●), H-Ni-SAL (●) and H-Mo-SAL (●) catalysts **c)** NH_3-TPD for the ZR (●) and H-NiMo-ZR (●) catalysts **d)** NH_3-TPD for the SZR (●) and H-NiMo-SZR (●) catalysts

AL, SAL and SZR display acidity in the weak and strong region according to the NH_3-TPD results (Figure 2). The ZR support exhibits no significant acidity, nor did its corresponding bimetallic catalysts (H-NiMo-ZR), as observed in Figure 2c and in Table 1 (*entries 7-8*). The DRIFT spectra for the AL, SAL and SZR depicted in Figure S1 indicate that the acidity of these supports is mainly of Lewis nature: the IR bands around 1450 cm^{-1} and 1610 cm^{-1} are associated with pyridine adsorbed on Lewis (L) acid sites. No bands around 1540 cm^{-1} associated with Brønsted (B) acid sites are found for any of the solids [35, 36]. The additional weak IR peak observed around 1495 cm^{-1} is normally attributed to a combination band associated with both B and L sites [36]. Thus, sulfating the alumina did not alter the nature of its acid sites. On the contrary, the zirconia experimented and increase in surface acidity due to the appearance of surface Lewis acid sites.

The NH_3-TPD results presented in Table 1 and Figure 2 also indicate that, in the case of the alumina, the sulfation process did not alter the strength and distribution of the Lewis sites either. Only a slight increase of weak acid sites is observed (0.420 mmol NH_3/g cat. for AL and 0.485 SAL mmol NH_3/g cat.). When compared with their corresponding bare supports, the bimetallic alumina catalyst H-NiMo-AL and H-NiMo-SAL display a larger amount of weak acid sites but a slightly smaller amount of strong acid sites.

As mentioned above sulfating the zirconia had a positive effect in the generation of acid sites, significantly increasing the Lewis acidity of the SZR support (Table 1). As depicted in Figure 2d, the majority of the acid sites found in the SZR support are weak. Its corresponding bimetallic catalysts, H-NiMo-SZR, also exhibits substantial acidity although the amount weak and strong acid sites is considerably smaller (Table 1).

3.1.3 ICP-AES

The Ni and Mo loadings shown in Table 1 are given in their oxide form, NiO and MoO_3, respectively. The nominal metal loadings are 5.0 % for the NiO and 12.0 % for the MoO_3. Two factors seem to affect the Ni content: the sulfation process and the type of support (i.e. alumina or zirconia). Higher amounts of Ni are observed for those catalysts based on zirconia (H-NiMo-ZR and H-NiMo-SZR) and for non-sulfated supports (H-NiMo-AL and H-NiMo-ZR). In the case of the Mo, the sulfation process is the most determinant factor: those non-sulfated supports (H-NiMo-AL and H-NiMo-ZR) give catalysts with higher Mo contents. Thus, the H-NiMo-ZR catalyst has the highest Ni loading followed by the H-NiMo-AL > H-NiMo-SZR >> H-NiMo-SAL. In the case of Mo, the highest loading is obtained for the H-NiMo-ZR followed by the H-NiMo-AL > H-NiMo-SAL > H-NiMo-SZR.

3.1.4 X-ray diffraction (XRD)

The diffractograms depicted for all the alumina catalysts (AL, H-NiMo-AL and SAL, NiMo-SAL and H-NiMo-SAL), are identical (Figure 3a and 3b). The main peaks corresponding to γ-Al_2O_3 phase are found at 2θ angles of 37.4, 45.9° and 66.7° (Powder Diffraction File (PDF): 01-074-2206). On the contrary, the diffractograms of the non-sulfated zirconia catalyst (ZR and H-NiMo-ZR) differ from the sulfated zirconia catalysts (SZR and H-NiMo-SZR) as depicted in Figure 3c and 3d. Both ZR and SZR diffractograms show broad peaks at 30.3°, 35.2°, 50.4° and

60.2° corresponding to tetragonal ZrO_2 (PDF: 01-088-1007), while the peaks at 24.2°, 28.2°, 31.5°, 34.4°, 40,7° and 50.4° are associated to the monoclinic ZrO_2 phase (PDF: 01-088-2390) [37]. The semi-quantitative analysis of the relative abundance of the zirconia phases was carried out based on the reference intensity ratio (RIR) for the most intense monoclinic and tetragonal peaks. The ZR support is about 20 % of tetragonal zirconium oxide and about 80 % monoclinic zirconium oxide, whereas in the SZR support the percentage of tetragonal phase is significantly higher, 70 %. This is in accordance with previous studies [36, 38] claiming that the presence of sulfate retards the conversion of the tetragonal phase to the monoclinic form.

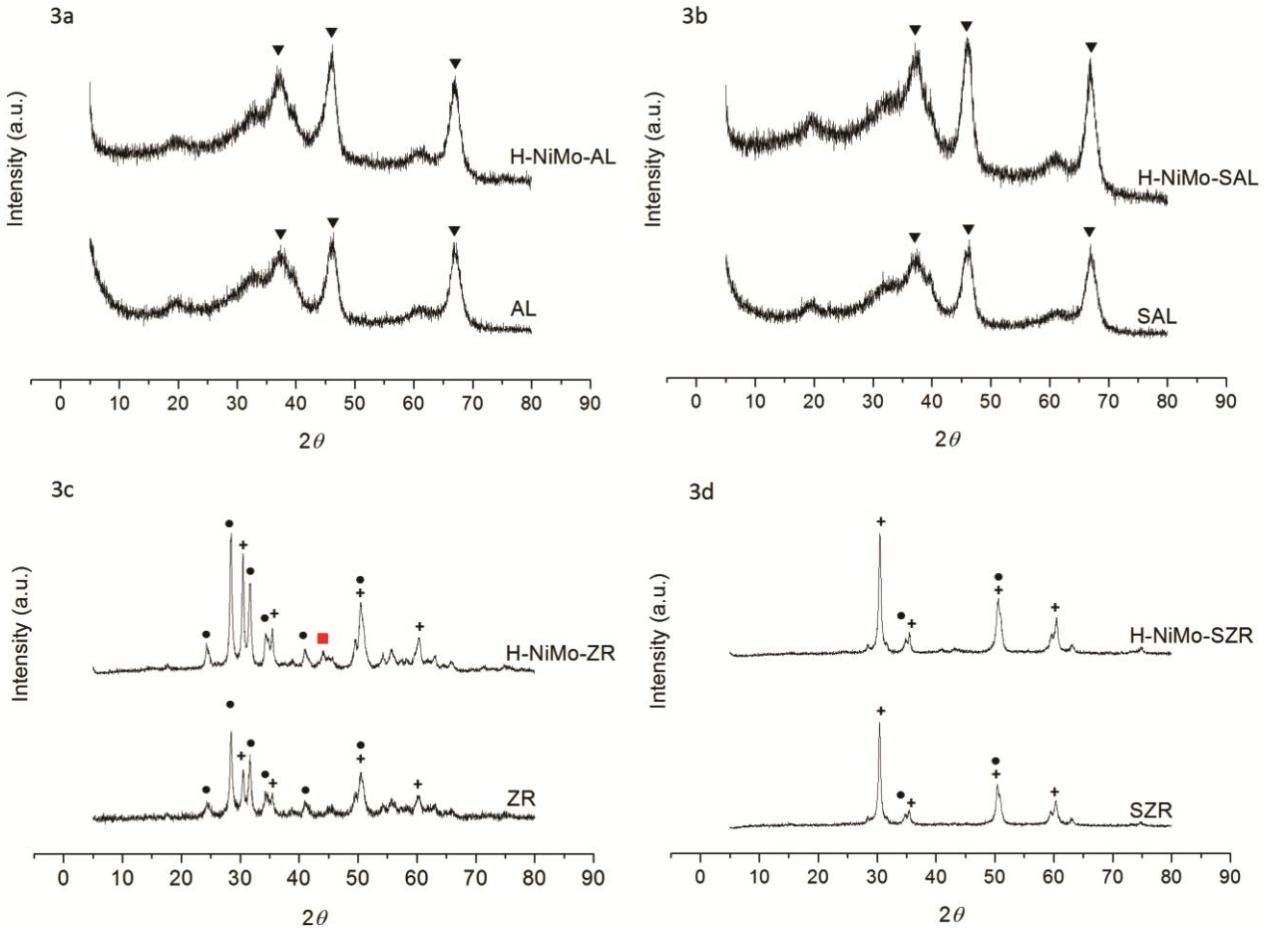

Figure 3a) XRD difractrograms for the AL and H-NiMo-AL **b)** XRD difractrograms for the SAL and H-NiMo-SAL **c)** XRD difractrograms for the ZR and H-NiMo-ZR and **d)** XRD difractrograms for the SZR and H-NiMo-SZR. (▼) Al_2O_3, (●) monoclinic ZrO_2, (+) tetragonal ZrO_2, (■) Ni.

Due to the quite low Ni and Mo loadings, identification of chemical phases related to Mo, MoO_x, Ni, NiO or even of $NiMoO_4$ species are not expected. The XRD patterns show no Ni (reflections at 2θ of 44.2°, 51.9°, and 76.1°; PDF: 01-087-0712), NiO (43.6° and 63.2°; PDF#: 01-078-0), Mo (40.5° and 73.7°; PDF: 00-042-1120), MoO_3 (27.3°; PDF: 00-001-0706), and $NiMoO_4$ (14.3° and 28.8°; PDF: 00-033-0948) characteristic reflections. Since crystalline particles of sizes below 2-4 nm are undetectable by the XRD technique, most likely these species give rise to very small coherent domains that are homogenously dispersed thought the support matrix or are amorphous. Only, the H-NiMo-ZR catalyst exhibits a characteristic peak for Ni at 2θ of 44.2° (Figure 3c).

3.1.5 Temperature-programmed reduction (TPR)

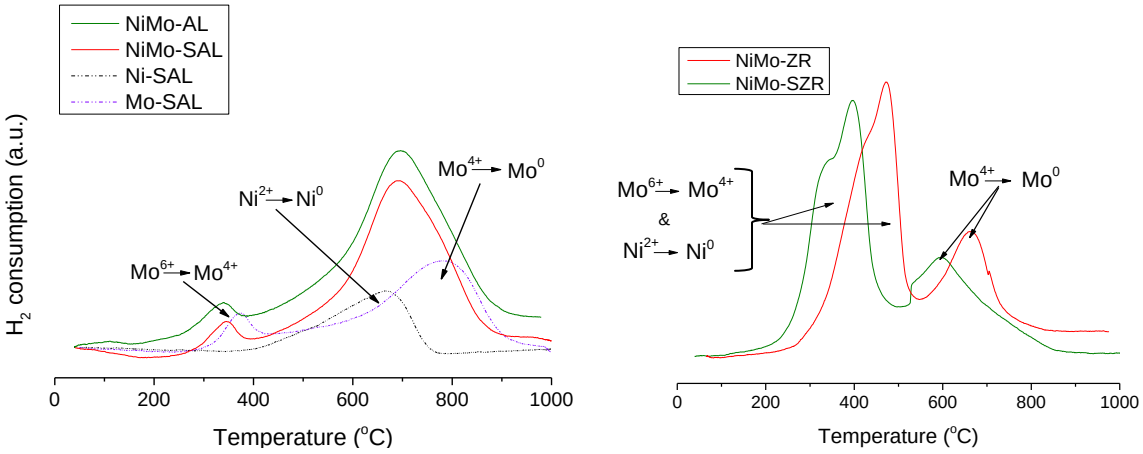

Figure 4a) TPR profile for the NiMo-AL (●), NiMo-SAL (●), Ni-SAL (●) and Mo-SAL (●) catalysts **b)** TPR profile for the NiMo-ZR (●) and NiMo-SZR (●) catalysts

Six solids (NiMo-AL, NiMo-SAL, NiMo-ZR, NiMo-SZR , Ni-SAL and Mo-SAL) corresponding to the non-pre-reduced bimetallic and monometallic catalysts (H-NiMo-AL, H-NiMo-SAL, H-NiMo-ZR, H-NiMo-SZR , H-Ni-SAL and H-Mo-SAL, respectively) were characterized by TPR (see Temperature-program-reduction (TPR), *Supplementary Information*). The TPR profiles of the analyzed solids are presented in Figure 4. No significant differences are observed in the shape of the NiMo-AL and NiMo-SAL TPR profiles (Figure 4a). The lower amount of hydrogen consumption observed for the NiMo-SAL can be related to the lower Ni and Mo loading (*Section 3.1.3*). Thus, sulfating the alumina did not affect significantly the reducibility of the metal species. Both catalysts show two main reduction peaks: a low temperature peak centered around 338-344 °C and high temperature broad peak centered at 671-672 °C. The low temperature peak

corresponds to the partial reduction (Mo^{6+} in Mo^{4+}) of amorphous, highly defective, multilayered Mo oxides or heteropolymolybdates (octahedral Mo species) [39, 40]. The high temperature peak is assigned to a combination of the reduction of Ni^{2+} in Ni^0 (400-750 °C temperature range) and Mo^{4+} in Mo^0 (centered around 800 °C), as in can be deduced from the TPR profiles obtained for the monometallic Ni-SAL and Mo-SAL catalysts (Figure 4a).

The TPR profiles for the NiMo-ZR and NiMo-SZR (Figure 4b) show that the zirconia support favors the reducibility of the metal species in comparison to the alumina. Both TPR-profiles exhibit comparable shapes. However, the reduction peaks for the NiMo-SZR catalyst are shifted to lower temperatures when compared to the ones for NiMo-ZR, indicating that sulfating the zirconia further decreases the reduction temperature of the Ni and Mo species. The TPR profiles comprise of a complex peak with two maxima and a simple peak, indicating three main reduction processes. According to the literature Ni/ZrO_2 TPRs mainly consist of a reduction temperature peak around 325-475 °C temperature range [41-43]. According to Gutierrez et al. [44] monometallic Mo/ZrO_2 catalysts exhibit two reduction peaks: a lower temperature peak centered around 350 °C corresponding to the reduction of Mo^{6+} to Mo^{4+}, and a high temperature peak centered around 500 °C corresponding to the reduction of Mo^{4+} to Mo^0. Thus, the first complex peak corresponds to the reduction of both Mo^{6+} to Mo^{4+} and Ni^{2+} to Ni^0 while the high temperature reduction peak corresponds to the reduction of Mo^{4+} to Mo^0, as previously observed in the literature [45].

3.1.6 Chemisorption

In this work, the CO-chemisorption technique is employed to determine the number of Ni active sites (given as μmol of CO/g) which is typically related to its catalytic activity (Table 1). The number of Ni active sites is strongly affected by the type of support and sulfation process, the former being the most relevant factor. Alumina supports show a higher dispersion of Ni, so does the non-sulfated supports. Hence, the highest number of active sites is found for the H-NiMo-AL catalyst with $18.5 \cdot 10^{-3}$ mmol CO/g cat. Values comparable in magnitude are observed for the H-NiMo-SAL catalyst with $6.9 \cdot 10^{-3}$ mmol CO/g cat. Conversely, the dispersion and number of Ni active sites for the zirconia catalysts iss poor: $2.1 \cdot 10^{-3}$ mmol CO/g cat for the H-NiMo-ZR and $0.7 \cdot 10^{-3}$ mmol CO/g cat for the H-NiMo-SZR.

3.2 Catalyst effects in LtL conversion

All the experiments were carried out twice. The results shown in Table 2 correspond to the average values of the replicates. When the oil and/or solid yield values differed more than 3.0 percentage points (mass fraction % points), an additional experiment was carried out. Table S3 (*Supplementary Information*) shows the oil and solid yield obtained for the replicates carried out with the bimetallic catalysts (i.e. H-NiMo-AL, H-NiMo-SAL, H-NiMo-ZR and H-NiMo-SZR). No significant differences are observed within the replicates, which confirms that the catalytic LtL experiments are highly reproducible. Note that the content of inorganic ashes of the rice straw lignin used for the LtL experiments is 14.9 % (mass); therefore, the actual organic solid yield, re-polymerized lignin fragments, is considerably smaller than the solid yield shown in the Table 2.

The recovery yield presented in Table 2 indicates the amount of lignin that has been converted into either oil or solid residue. It is also an indirect measurement of the amount of lignin converted to gas and/or the oil and solid that may have been lost during the work-up procedure.

Table 2: Oil, solid and lignin recovery yield, and elemental analysis and M_w of the oils for the catalytic and non-catalytic experiments

Entry	Experiment[a]	Oil Yield[b]	Solid Yield[b]	Lignin recovery yield[b]	H/C[b]	O/C[b]	M_w[b] (Da)
		(mass %)[c]			molar ratio		
1	**NC**	36.0	43.5	79.5	1.27	0.13	347
2	**AL**	50.7	27.0	77.7	1.18	0.14	415
3	**SAL**	52.0	27.6	79.6	1.17	0.14	382
4	**ZR**	37.2	32.2	69.4	1.23	0.13	373
5	**SZR**	41.1	34.8	76.0	1.22	0.14	363
6	**H-NiMo-AL**	63.7	19.6	83.3	1.22	0.14	410
7	**H-NiMo-SAL**	64.8	18.7	83.5	1.22	0.14	371
8	**H-NiMo-ZR**	61.2	20.0	81.2	1.26	0.15	454
9	**H-NiMo-SZR**	61.9	17.3	79.2	1.25	0.16	421
10	**NiMo-SAL**	60.2	23.8	84.0	1.22	0.15	387
11	**NiMo-SZR**	57.5	25.2	82.7	1.26	0.13	355

[a] **NC:** refers to non-catalyzed experiment **H** refers to those catalyst that were submitted to a pre-reduction treatment, **NiMo:** bimetallic catalysts containing Ni and Mo, **Ni:** monometallic catalyst containing only Ni, **Mo:** monometallic catalyst containing only Mo, **AL:** γ-alumina, **SAL:** sulfated alumina, **ZR:** zirconia

and **SZR:** sulfated zirconia [b] Average value of the results obtained in the replicates [c] Relative to the lignin input

3.2.1 Effect of the bare support (AL, SAL, ZR and SZR)

The results obtained with the bare supports are compared with the ones obtained for the non-catalyzed (NC) experiment (*entries 1-5*, Table 2). The lignin recovery yields are above a mass fraction of 75 % except for the ZR experiment, meaning that for this experiment a higher amount of oil or solid was either gasified or lost during the work-up procedure.

Only the alumina supports (AL and SAL) exhibit catalytic activity towards the de-polymerization of lignin. The highest oil yield, with a mass fraction of 52.0 %, is obtained for the SAL followed closely by the AL support (Figure 5). The oil yield of the zirconia supports (ZR and SZR) is only slightly higher than the non-catalyzed (NC) experiment, confirming their lack of activity.

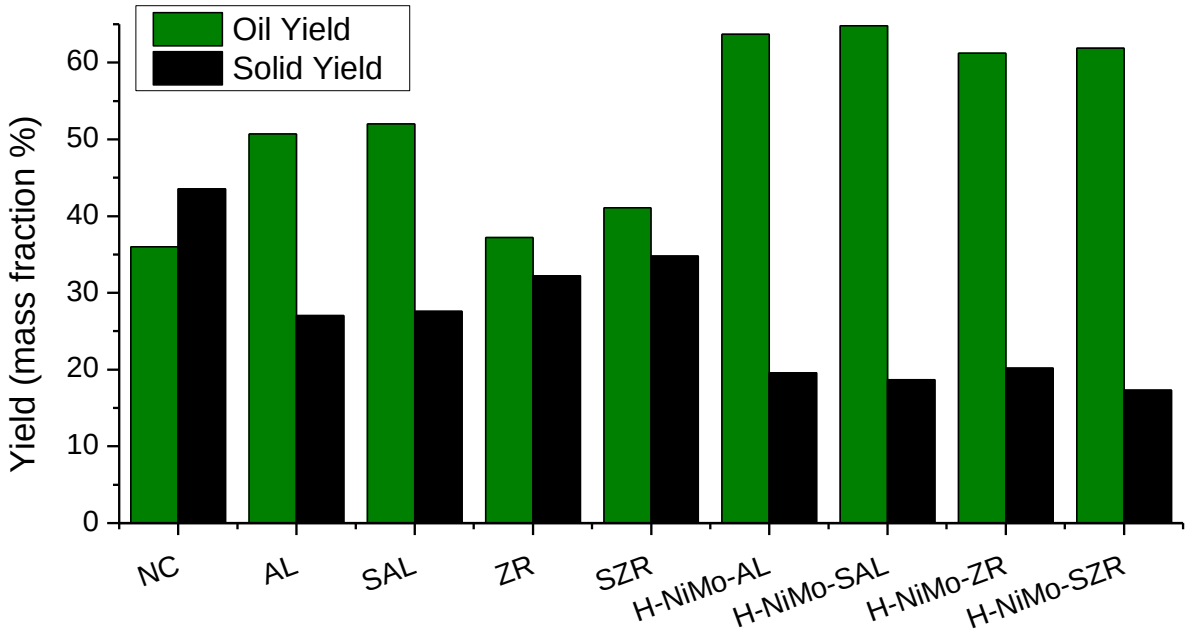

Figure 5: Oil and solid yield for bare supports (NC, AL, SAL, ZR and SZR) and the H-NiMo-AL, H-NiMo-SAL, H-NiMo-ZR and H-NiMo-SZR catalysts. Experiments at 340 °C and 6 h. The oil and solid yield are given in mass fraction %.

Table S4 (*Supplementary Information*) shows the relative abundance of the main lignin-derived compounds present in the oils. Alkyl substituted phenols are the dominant components. No highly oxygenated compounds, such as substituted guaiacols or catechols, are found; the most oxygenated compounds are ethyl benzoate (EB ether), small amounts of ethoxyphenol (EtPh) and some high molecular weight methoxy- and hydroxy- substituted alkylphenols. Additional intense peaks corresponding to 4-hydroxy-butanoic acid and alkyl esters are also found. It is believed that these compounds are formed due to chemical reactions between formic acid, ethanol and lignin degradation products with the gas components (mainly H_2 and CO_2 produced from the decomposition of formic acid). When comparing the NC oil with those produced in the presence of the bare supports (AL, SAL, ZR and SZR), it is clear that the latter contain a higher amount of highly alkylated single ring phenolics, especially a higher amount of highly alkylated methoxy- and hydroxy-phenols. This suggests that the supports increase the alkylation rate of the monomers. The type of support does not seem to affect significantly the relative amount and type of compounds.

3.2.2 Effect of the bimetallic catalysts (H-NiMo-AL, H-NiMo-SAL, H-NiMo-ZR and H-NiMo-SZR)

The bimetallic catalysts (H-NiMo-AL, H-NiMo-SAL, H-NiMo-ZR and H-NiMo-SZR) exhibit higher activities than their corresponding bare supports: Ni and Mo metallic phases significantly increase the oil yields while decreasing the solid yields for all the catalysts studied (*entries 6-9*, Table 2 and Figure 5). The lignin recovery yields also increase to around a mass fraction of 80 %.

All the catalysts exhibit similar activities regardless the type of support. The highest oil yield, given as mass fraction %, is obtained for the H-NiMo-SAL (64.8 %), followed closely by the H-NiMo-AL (63.7 %) > H-NiMo-SZR (61.9 %) > H-NiMo-ZR (61.2 %). The solid yields obtained are also significantly lower: all the catalysts give similar solid yields ranging from 17.3 % for the H-NiMo-SZR to 20.0 % for the H-NiMo-ZR (Table 2).

The bimetallic catalysts yield oils with slightly higher H/C molar ratios than their corresponding bare supports; the O/C molar ratios are comparable or slightly higher (*entries 2-9*, Table 2). The average molecular weight of the oil (M_w) decreases slightly in the case of the alumina-based catalysts (H-NiMo-AL and H-NiMo-SAL), but increases considerably for the zirconia-based ones (H-NiMo-ZR and H-NiMo-SZR). Small differences are also observed in

terms of composition of the oils when compared the bimetallic catalyst with the bare supports (Table S4, *Supplementary Information*). The bimetallic catalysts yield oils containing propofol (Prop) and 2-(1,1-dimethylethyl)-3-methylphenol ((dME)MPh); while other compounds such as 2,3,5-trimethyl-1,4-benzenediol ((dME)dHB) and 4-(1,1-dimethylethyl)-1,2-benzenediol (dMdMB) are no longer observed. The bimetallic catalysts also produce oils with a larger content of diethyl-phenol (dEPh). Thus, the bimetallic catalyst still yield a higher amount of highly alkylated single ring phenolics when compared with the NC oil.

In order to evaluate the effect of pre-reducing (activating) the bimetallic catalyst, two additional experiments were carry out with non-pre-reduced catalysts, i.e. NiMo-SAL and NiMo-SZR (entries 10-11, *Supplementary Information*). These catalysts are the non-pre-reduced counterparts of the most active alumina and zirconia catalysts. The NiMo-SAL and NiMo-SZR catalysts present similar textural (Table S5 and Figure S2) and acidic properties (Table S5 and Figure S3) when compared to their pre-reduced H-NiMo-SAL and H-NiMo-SZR counterparts, although the NiMo-SAL and NiMo-SZR present a larger amount of weak Lewis acid sites. The results presented in Table 2 (*entries 10-11*) show that the oil yields of the non-pre-reduced NiMo-SAL and NiMo-SZR are slightly lower than the ones obtained for their pre-reduced counterparts; the solid yields are slightly higher. For the sulfated alumina catalysts (H-NiMo-SAL and NiMo-SAL), the H/C, O/C and M_w values of the oils are comparable, while in the case of the sulfated zirconia catalysts (H-NiMo-SZR and NiMo-SZR), only the M_w values differ.

3.2.3 Effect of the Ni and Mo

In this section, the activities of monometallic H-Ni-SAL and H-Mo-SAL catalysts are compared with the activity of the bimetallic H-NiMo-SAL catalyst in order to evaluate the role of the Ni and Mo species (Table 3). All the three catalysts are based on the same sulfated alumina support (SAL). The experiments described in this section were performed one year after the ones described in previous sections. Thus, the baseline H-NiMo-SAL experiment was again repeated to take into account the effect of the chemical and physical transformations of lignin upon storage or other serendipity factors. This experiment is labeled R1-NiMo-SAL. The yields are somewhat different, with the oil yield increasing from 64.8 to 76.5 %, but retaining comparable elemental ratios and M_w values.

Table 3: Oil, solid and lignin recovery yield, and elemental analysis and M_w of the oils for the monometallic catalysts and recycled H-Ni-Mo-SAL catalyst.

Experiment[a]	Type of catalyst	Oil Yield[b]	Solid Yield[b]	Lignin recovery yield[b]	H/C[b]	O/C[b]	M_w[b] (Da)
		(mass %)			molar ratio		
NC	-	36.0	43.5	79.5	1.27	0.13	347
H-Ni-SAL	Monometallic Ni	72.5	22.4	94.9	1.24	0.15	428
H-Mo-SAL	Monometallic Mo	64.0	31.1	95.1	1.31	0.13	436
ASH	Lignin ashes	42.4	48.5	90.9	1.30	0.13	326
R1-NiMo-SAL	Bimetallic NiMo (fresh, 1st test)	76.5	19.3	95.8	1.22	0.15	397
R2-NiMo-SAL	Bimetallic NiMo (2nd test)	72.7	24.3	97	1.25	0.13	398
R3-NiMo-SAL	Bimetallic NiMo (3rd test)	76.5	21.6	98.1	1.24	0.13	391

[a] **NC:** refers to non-catalyzed experiment **ASH:** inorganic ash catalysed experiment, **R1**: experiment with the fresh bimetallic H-NiMo-SAL catalyst, 1st test. **R2:** recycled H-NiMo-SAL bimetallic catalyst 2nd test and **R2**: recycled H-NiMo-SAL bimetallic catalyst 3rd test [a] Average molecular weight of the oil [b] Average value of the results obtained in the replicates [c] Relative to the lignin input

The results depicted in Figure 6 and Table 3 show that the bimetallic catalyst (R1-NiMo-SAL experiment) gives the highest oil and lowest solid yields, a mass fraction of 76.5 % and 19.3 %, respectively. Still, the oil and solid yields of the monometallic Ni catalyst (H-Ni-SAL) are similar to the ones obtained for the bimetallic R1-NiMo-SAL catalyst, a mass fraction 72.5 % and 22.4 %, respectively. The monometallic Mo catalyst (H-Mo-SAL), on the contrary, gives a relatively lower oil yield, mass fraction of 64.0 %, and significantly higher solid yield, mass fraction of 31.1 %. Considerable differences in the properties of the oils are also found (Table 3). The H-Mo-SAL oil has a higher H/C and a lower O/C ratio than the H-Ni-SAL and R1-NiMo-SAL oil; thus, the monometallic H-Mo-SAL catalyst produces a more hydrodeoxygenated oil. In terms of M_w, the lowest values were obtained for the bimetallic R1-NiMo-SA catalyst (397 Da) followed by the monometallic H-Ni-SAL (428 Da) and the H-Mo-SAL (436 Da).

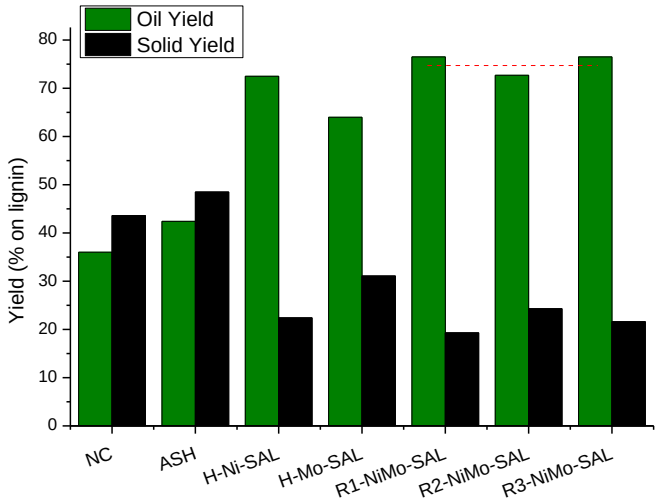

Figure 6 oil and solid yield for the NC, ASH, H-Ni-SAL, H-Mo-SAL, R1-NiMo-SAL, R2-NiMo-SAL and R3-NiMo-SAL experiments

Differences in the oil composition are also found between the monometallic catalysts (Table S6, *Supplementary Information*). In general, the H-Mo-SAL oil has a higher abundance of alkylated phenols such as ethylmethylphenol (EMPh), diethyl phenol (dEPh) and propofol (Prop); while the H-Ni-SAL oil contains methoxy- substituted compounds such as 1-ethoxy-2-methoxy-4-methylbenzene (EtMtMB) and 4-methoxy-2,3,6-trimethyl-phenol (Mt-tMPh), and a larger amount of ethoxyphenol (EtPh). This is in accordance with the elemental analysis and explains the higher H/C and lower O/C ratios obtained for the H-Mo-SAL catalyst.

3.2.4 Recyclability of the H-NiMo-SAL catalyst (R1-NiMo-SAL)

In *Section 3.2.2*, the H-NiMo-SAL was found to be the best catalyst in terms of oil yield and oil properties. Thus, the recyclability of the H-NiMo-SAL catalyst was studied for three consecutive catalytic tests. The experiments are summarized in Table 3 and Figure 6. Note that the R1-NiMo-SAL experiment corresponds to the experiment carried out with the fresh H-NiMo-SAL catalyst as described in the previous section. The R2-NiMo-SAL and R3-NiMo-SAL experiments correspond the second and third test, respectively.

The catalyst was recycled together with the inorganic lignin ashes. Hence, the possible catalytic effect of the inorganic ashes is first evaluated (ASH) in order to subtract this effect from the results obtained upon recycling. The composition of the ashes had been also determined by ICP-MS to connect their possible activity to specific metal species (Table S7, *Supplementary*

Information). The ASH experiment gives not only slightly higher oil but also higher solid yield than the NC counterpart (Table 3) does. Thus, the ashes seemed to reduce the amount of oil and solid lost during the work-up procedure. There was also an increase in the H/C ratio and a slight decrease in the M_w value of the oil. This could be assigned to the presence of either Fe or Si inorganic species, since the rest of the elements found were in negligible concentrations. However, as observed in Table 3 the activity of the inorganic lignin ashes was insignificant in comparison to the bimetallic H-NiMo-SAL catalyst.

All the recyclability tests (Table 3) give similar lignin recovery yields, ranging from a mass fraction of 95.8 % for the R1-NiMo-SAL experiment to 98.1 % for the R3-NiMo-SAL. Regarding the oil yield, no significant decrease after three consecutive tests is observed. A slight oil decrease is detected after the first test (from a mass fraction of 76.5 % for the R1-NiMo-SAL to 72.7 % for the R2-NiMo-SAL), but the oil yield increases again in the third test up to a mass fraction of 76.5 %. The opposite trend is observed for the solid yield: after the first test, the solid yield increases from a mass fraction of 19.3 % for the R1-NiMo-SAL to 24.3 % for the R2-NiMo-SAL, but decreases to 21.6 % for the R3-NiMo-SAL. In terms of elemental analysis, the H/C ratio increases after each test (from 1.22 to 1.24 and 1.25) and the O/C ratio decreases (from 0.15 to 0.13) which could be assigned to the effect of the inorganic ashes. The M_w value does not vary.

4. Discussion

As it has been described in the introduction, the conversion of lignin in a formic acid/ethanol medium follows the general reaction pathway depicted in Scheme 1 [25]. Comparable sequential reaction schemes have already been reported for the conversion of lignin in reductive environments [46-51]. Initially, lignin is fragmented into smaller lignin species, both mono- and oligomers, through the cleavage of its aliphatic ether bonds (i.e. de-polymerization). These lignin fragments (oligomers) can further undergo de-polymerization, HDO and alkylation reactions, and/or re-polymerization into char. The hydrodeoxygenated and alkylated lignin fragments exhibit higher chemical stabilities and show lower tendency towards re-polymerization [47, 48, 51]. Particularly, in a formic acid/ethanol medium, the aliphatic ether bond cleavage (de-polymerization) is believed to occur through a formylation-deformylation-hydrogenolysis mechanism, where the hydrogenolysis step is catalyzed by a metallic active site [25].

Interestingly, the results presented in *Section 3.2.1* prove that the aliphatic ether bond cleavage, *i.e.* lignin de-polymerization, can be catalyzed in the absence of metallic species. Both of the bare alumina supports (AL and SAL) increased the oil and decreased the solid yield indicating that larger amounts of lignin fragments were produced. The results presented in *Section 3.2.1* also prove that less acidic SZR and the non-acidic ZR exhibited no significant activity. This indicates that only strong Lewis acid sites are able to catalyze the de-polymerization of lignin. Both AL and SAL support exhibited high concentration of strong Lewis acid sites, while the less acidic SZR support contained mainly weak Lewis acid sites.

Nevertheless, the activity of the strong Lewis acid sites in the aliphatic ether bond cleavage seems irrelevant when compared to the activity of the metallic species: substantially higher oil and lower solid yields are obtained with the bimetallic catalyst in comparison to the bare supports. The relevance of the metal catalyzed mechanism is particularly evident when comparing the zirconia and alumina catalysts: the ZR and SZR bare supports exhibit no catalytic activity when compared to the AL and SAL; however, the bimetallic H-NiMo-ZR and H-NiMo-SZR catalysts exhibit activities comparable to the bimetallic alumina catalysts (H-NiMo-AL and H-NiMo-SAL). The dominance of the metal catalyzed aliphatic ether bond cleavage over the acid catalyzed aliphatic ether bond cleavage has already been reported in hydrogen/water media [52].

The elemental analysis, GPC-SEC and GC-MS analysis of the oils also point towards this conclusion. Despite exhibiting different surface acidities, all the bimetallic catalysts produce oils with comparable H/C, O/C and M_w values and oil compositions (Section 3.2.2). Thus, the metal catalyzed aliphatic ether bond cleavage seems to be the dominant reaction mechanism, regardless the type of support. The elemental analysis also indicates that the presence of metallic species have an effect on the properties of the oils, increasing their H/C ratio. The GC-MS analysis of the oils support the proposition that the bare supports and their corresponding bimetallic catalysts are able to increase the abundance of alkylated compounds. Catalytic alkylation could also contribute to the oil yield increase through the stabilization of the lignin monomers [47], although this contribution is believed to be secondary [51].

To evaluate the distinctive role of the Ni and Mo metallic species in the LtL conversion mechanism additional experiments with monometallic H-Ni-SAL and H-Mo-SAL catalyst were carried out. The results in Section 3.2.3 show that the oil and solid yields obtained for the monometallic Ni catalysts (H-Ni-SAL) are comparable to the ones obtained for the bimetallic NiMo catalyst (R1-NiMo-SAL/H-NiMo-SAL); the monometallic Mo catalysts (H-Mo-SAL), however, gives significantly lower oil and higher solid yields. All this suggests that the Ni species are more active towards aliphatic ether bond cleavage than Mo species (Scheme 1). Conversely, the monometallic Mo catalysts is more active towards HDO of the lignin fragments in comparison to the monometallic Ni catalyst: the H-Mo-SAL catalyst yielded oil with higher H/C and lower O/C ratios and a lower number of oxygenated aromatics when compared with the H-Ni-SAL. This is in accordance with previous studies with lignin model compounds: Ni^0 is known to catalyze the cleavage of aryl ether bonds, while MoO_3 is known to cleavage preferentially phenolic C-O bonds over weaker aliphatic ether bonds [12, 53, 54].

Non-pre-reduced NiMo-SAL and NiMo-SZR catalysts exhibit similar activities when compared to their pre-reduced H-NiMo-SAL and H-NiMo-SZR counterparts (Section 3.2.2), which indicates that the LtL environment is able to produce Ni^0 species *in situ*. In order to prove this hypothesis, two non-pre-reduced catalysts, monometallic Ni-SAL and bimetallic NiMo-SAL, were submitted to the LtL environment in the absence of lignin. These catalysts are named Ni-SAL-Used and NiMo-SAL-Used, and their TPR profiles were compared with fresh Ni-SAL and NiMo-SAL (Figure S4). The TPR results confirm that the LtL environment is able to reduce Ni^{2+} to Ni (0). The hydrogen consumption for the fresh Ni-SAL catalyst was 1.061 mmol of H_2/g catalysts, while only 0.5715 mmol of H_2/g catalysts for the used Ni-SAL (*see* TPR analysis, Supplementary Information). A lower H_2 consumption is also observed in the case of the bimetallic catalysts: the hydrogen consumption of the fresh NiMo-SAL is 2.262 mmol of H_2/g catalysts, while in the case of the used NiMo-SAL the hydrogen consumption is 1.306 mmol of H_2/g catalysts.

The BET (see Section 3.1.1) and CO-chemisorption (see Section 3.1.6) analysis indicate, however, that not all the Ni species participate to the same extent in the catalytic aliphatic ether bond cleavage. The bimetallic alumina catalysts (H-NiMo-AL and H-NiMo-SAL) exhibit a considerably higher porosity and number of Ni active sites as compared to the bimetallic zirconia catalysts (H-NiMo-ZR and H-NiMo-SZR). Furthermore, the low porosity of the bimetallic

zirconia catalysts indicates that in the H-NiMo-ZR and H-NiMo-SZR most of the Ni species are found over the outer surface of the supports. Given the comparable oil and solid yield obtained for all the bimetallic catalysts, it is believed that the aliphatic ether bond hydrogenolysis is mainly catalyzed by the outer Ni^0 species. Only the Ni^0 species of the outer surface of the catalyst could interact with the high molecular weight and voluminous lignin fragments. Those Ni species within the pores, on the contrary, could only interact with the smaller lignin monomers.

When studying the recyclability of the H-NiMo-SAL catalyst, no deactivation is observed after three consecutive tests. The inorganic ashes do not display a significant catalytic activity in terms of oil and solid yield although they do have an effect on the H/C and O/C ratios.

5. Conclusion

The role of Ni, Mo and the acid sites on the overall reaction mechanism of the catalytic LtL conversion in formic acid/ethanol media have been studied. The oil yield and its properties are the product of a combination of successive catalytic reactions. Initially, lignin is de-polymerized into smaller fragments through the cleavage of the aliphatic ether bonds. These fragments can further undergo HDO and alkylation reactions which hinders their repolymerization into char. The results suggest that the catalytic aliphatic ether bond cleavage contributes to a larger extend than catalytic HDO and alkylation reactions to the production of bio-oil. The contribution of the HDO and alkylation reactions is secondary in the case of the oil yield, but do have an effect on the oil properties and compositions.

In the absence of metallic species strong Lewis acid sites are able to catalyze the initial aliphatic ether bond cleavage. In the presence of metals (i.e. Ni and Mo), in contrast, the metal catalyzed aliphatic ether bond cleavage mechanism prevails over the acid catalyzed mechanism. Ni^0, particularly those metallic Ni active sites found in the outer surface of the catalyst, are found to be more active than Mo species in the catalytic ether bond cleavage. In contrast, Mo was found to be more active for HDO reactions. All the bimetallic catalysts also exhibited significant activity towards catalytic alkylation.

6. Acknowledgements

This project was supported by the Lignoref project group (including The Research Council of Norway (grant no.190965/S60), Statoil ASA, Borregaard AS, Allskog BA, Cambi AS,Xynergo AS/Norske Skog, Hafslund ASA and Weyland AS) and by the Swedish Energy Agency and by VR and VINNOVA. The authors would also like to thank I. J. Fjellanger, Mali H. Rosnes, and Ainhoa Ocio for their assistance in the characterization of the oil and catalysts, and the Technical College of Bergen for supplying lignin. SGIker technical and human support (UPV/EHU, MINECO, GV/EJ, ERDF and ESF) is also gratefully acknowledged.

7. References

[1] Y. Zheng, C. Yu, Y.-S. Cheng, C. Lee, C.W. Simmons, T.M. Dooley, R. Zhang, B.M. Jenkins, J.S. VanderGheynst, Integrating sugar beet pulp storage, hydrolysis and fermentation for fuel ethanol production, Applied Energy, 93 (2012) 168-175.
[2] S. Tian, J. Zhu, X. Yang, Evaluation of an adapted inhibitor-tolerant yeast strain for ethanol production from combined hydrolysate of softwood, Applied Energy, 88 (2011) 1792-1796.
[3] S.I. Mussatto, E.M.S. Machado, L.M. Carneiro, J.A. Teixeira, Sugars metabolism and ethanol production by different yeast strains from coffee industry wastes hydrolysates, Applied Energy, 92 (2012) 763-768.
[4] R. Sahu, P.L. Dhepe, A One-Pot Method for the Selective Conversion of Hemicellulose from Crop Waste into C5 Sugars and Furfural by Using Solid Acid Catalysts, ChemSusChem, 5 (2012) 751-761.
[5] R.J.A. Gosselink, E. de Jong, B. Guran, A. Abächerli, Co-ordination network for lignin—standardisation, production and applications adapted to market requirements (EUROLIGNIN), Industrial Crops and Products, 20 (2004) 121-129.
[6] M. Kleinert, T. Barth, Phenols from Lignin, Chemical Engineering & Technology, 31 (2008) 736-745.
[7] M. Kleinert, J.R. Gasson, T. Barth, Optimizing solvolysis conditions for integrated depolymerisation and hydrodeoxygenation of lignin to produce liquid biofuel, Journal of Analytical and Applied Pyrolysis, 85 (2009) 108-117.
[8] L.J. Jönsson, B. Alriksson, N.-O. Nilvebrant, Bioconversion of lignocellulose: inhibitors and detoxification, Biotechnology for Biofuels, 6 (2013) 1-10.
[9] D.J. Hayes, S. Fitzpatrick, M.H.B. Hayes, J.R.H. Ross, The Biofine Process – Production of Levulinic Acid, Furfural, and Formic Acid from Lignocellulosic Feedstocks, Biorefineries-Industrial Processes and Products, Wiley-VCH Verlag GmbH2005, pp. 139-164.
[10] M. Oregui Bengoechea, A. Hertzberg, N. Miletić, P.L. Arias, T. Barth, Simultaneous catalytic de-polymerization and hydrodeoxygenation of lignin in water/formic acid media with Rh/Al2O3, Ru/Al2O3 and Pd/Al2O3 as bifunctional catalysts, Journal of Analytical and Applied Pyrolysis, 113 (2015) 713-722.
[11] L. Liguori, T. Barth, Palladium-Nafion SAC-13 catalysed depolymerisation of lignin to phenols in formic acid and water, Journal of Analytical and Applied Pyrolysis, 92 (2011) 477-484.
[12] C. Li, X. Zhao, A. Wang, G.W. Huber, T. Zhang, Catalytic Transformation of Lignin for the Production of Chemicals and Fuels, Chemical Reviews, 115 (2015) 11559-11624.
[13] Q. Song, F. Wang, J. Xu, Hydrogenolysis of lignosulfonate into phenols over heterogeneous nickel catalysts, Chemical Communications, 48 (2012) 7019-7021.

[14] C. Li, M. Zheng, A. Wang, T. Zhang, One-pot catalytic hydrocracking of raw woody biomass into chemicals over supported carbide catalysts: simultaneous conversion of cellulose, hemicellulose and lignin, Energy & Environmental Science, 5 (2012) 6383-6390.
[15] X. Wang, R. Rinaldi, Corrigendum: Solvent Effects on the Hydrogenolysis of Diphenyl Ether with Raney Nickel and their Implications for the Conversion of Lignin, ChemSusChem, 5 (2012) 1335-1335.
[16] V.N. Bui, D. Laurenti, P. Afanasiev, C. Geantet, Hydrodeoxygenation of guaiacol with CoMo catalysts. Part I: Promoting effect of cobalt on HDO selectivity and activity, Applied Catalysis B: Environmental, 101 (2011) 239-245.
[17] C. Zhao, J. He, A.A. Lemonidou, X. Li, J.A. Lercher, Aqueous-phase hydrodeoxygenation of bio-derived phenols to cycloalkanes, Journal of Catalysis, 280 (2011) 8-16.
[18] C. Zhao, J.A. Lercher, Selective Hydrodeoxygenation of Lignin-Derived Phenolic Monomers and Dimers to Cycloalkanes on Pd/C and HZSM-5 Catalysts, ChemCatChem, 4 (2012) 64-68.
[19] C. Zhao, Y. Kou, A.A. Lemonidou, X. Li, J.A. Lercher, Hydrodeoxygenation of bio-derived phenols to hydrocarbons using RANEY[registered sign] Ni and Nafion/SiO2 catalysts, Chemical Communications, 46 (2010) 412-414.
[20] D.D. Laskar, M.P. Tucker, X. Chen, G.L. Helms, B. Yang, Noble-metal catalyzed hydrodeoxygenation of biomass-derived lignin to aromatic hydrocarbons, Green Chemistry, 16 (2014) 897-910.
[21] W. Zhang, J. Chen, R. Liu, S. Wang, L. Chen, K. Li, Hydrodeoxygenation of Lignin-Derived Phenolic Monomers and Dimers to Alkane Fuels over Bifunctional Zeolite-Supported Metal Catalysts, ACS Sustainable Chemistry & Engineering, 2 (2014) 683-691.
[22] S.K. Singh, J.D. Ekhe, Towards effective lignin conversion: HZSM-5 catalyzed one-pot solvolytic depolymerization/hydrodeoxygenation of lignin into value added compounds, RSC Advances, 4 (2014) 27971-27978.
[23] X. Wang, R. Rinaldi, Bifunctional Ni catalysts for the one-pot conversion of Organosolv lignin into cycloalkanes, Catalysis Today, 269 (2016) 48-55.
[24] A. Kloekhorst, Y. Shen, Y. Yie, M. Fang, H.J. Heeres, Catalytic hydrodeoxygenation and hydrocracking of Alcell® lignin in alcohol/formic acid mixtures using a Ru/C catalyst, Biomass and Bioenergy, 80 (2015) 147-161.
[25] M. Oregui-Bengoechea, I. Gandarias, P.L. Arias, T. Barth, Unraveling the Role of Formic Acid and the Type of Solvent in the Catalytic Conversion of Lignin: A Holistic Approach, ChemSusChem, (2017) n/a-n/a.
[26] F. Babou, G. Coudurier, J.C. Vedrine, Acidic Properties of Sulfated Zirconia: An Infrared Spectroscopic Study, Journal of Catalysis, 152 (1995) 341-349.
[27] E. Zhao, Y. Isaev, A. Sklyarov, J.J. Fripiat, Acid centers in sulfated, phosphated and/or aluminated zirconias, Catalysis Letters, 60 (1999) 173-181.
[28] M.L. Guzmán-Castillo, E. López-Salinas, J.J. Fripiat, J. Sánchez-Valente, F. Hernández-Beltrán, A. Rodríguez-Hernández, J. Navarrete-Bolaños, Active sulfated alumina catalysts obtained by hydrothermal treatment, Journal of Catalysis, 220 (2003) 317-325.
[29] P. Priecel, L. Čapek, D. Kubička, F. Homola, P. Ryšánek, M. Pouzar, The role of alumina support in the deoxygenation of rapeseed oil over NiMo–alumina catalysts, Catalysis Today, 176 (2011) 409-412.
[30] G. Duan, C. Zhang, A. Li, X. Yang, L. Lu, X. Wang, Preparation and Characterization of Mesoporous Zirconia Made by Using a Poly (methyl methacrylate) Template, Nanoscale Research Letters, 3 (2008) 118-122.
[31] Y. Sun, S. Ma, Y. Du, L. Yuan, S. Wang, J. Yang, F. Deng, F.-S. Xiao, Solvent-Free Preparation of Nanosized Sulfated Zirconia with Brønsted Acidic Sites from a Simple Calcination, The Journal of Physical Chemistry B, 109 (2005) 2567-2572.
[32] M.K. Mishra, B. Tyagi, R.V. Jasra, Synthesis and characterization of nano-crystalline sulfated zirconia by sol–gel method, Journal of Molecular Catalysis A: Chemical, 223 (2004) 61-65.

[33] J.W. McBain, An Explanation of Hysteresis in the Hydration and Dehydration of Gels, Journal of the American Chemical Society, 57 (1935) 699-700.
[34] G. Mason, The effect of pore space connectivity on the hysteresis of capillary condensation in adsorption—desorption isotherms, Journal of Colloid and Interface Science, 88 (1982) 36-46.
[35] T.-s. Yang, T.-h. Chang, C.-t. Yeh, Acidities of sulfate species formed on a superacid of sulfated alumina, Journal of Molecular Catalysis A: Chemical, 115 (1997) 339-346.
[36] W.-H. Chen, H.-H. Ko, A. Sakthivel, S.-J. Huang, S.-H. Liu, A.-Y. Lo, T.-C. Tsai, S.-B. Liu, A solid-state NMR, FT-IR and TPD study on acid properties of sulfated and metal-promoted zirconia: Influence of promoter and sulfation treatment, Catalysis Today, 116 (2006) 111-120.
[37] G. Shi, F. Yu, Y. Wang, D. Pan, H. Wang, R. Li, A novel one-pot synthesis of tetragonal sulfated zirconia catalyst with high activity for biodiesel production from the transesterification of soybean oil, Renewable Energy, 92 (2016) 22-29.
[38] A. Corma, Inorganic Solid Acids and Their Use in Acid-Catalyzed Hydrocarbon Reactions, Chemical Reviews, 95 (1995) 559-614.
[39] L. Qu, W. Zhang, P.J. Kooyman, R. Prins, MAS NMR, TPR, and TEM studies of the interaction of NiMo with alumina and silica–alumina supports, Journal of Catalysis, 215 (2003) 7-13.
[40] M. Henker, K.-P. Wendlandt, J. Valyon, P. Bornmann, Structure of MoO3/Al2O3-SiO2 catalysts, Applied Catalysis, 69 (1991) 205-220.
[41] Á. Calafat, N. Sánchez, Production of carbon nanotubes through combination of catalyst reduction and methane decomposition over Fe–Ni/ZrO2 catalysts prepared by the citrate method, Applied Catalysis A: General, 528 (2016) 14-23.
[42] J. Ren, X. Qin, J.-Z. Yang, Z.-F. Qin, H.-L. Guo, J.-Y. Lin, Z. Li, Methanation of carbon dioxide over Ni–M/ZrO2 (M = Fe, Co, Cu) catalysts: Effect of addition of a second metal, Fuel Processing Technology, 137 (2015) 204-211.
[43] Z. Li, X. Hu, L. Zhang, S. Liu, G. Lu, Steam reforming of acetic acid over Ni/ZrO2 catalysts: Effects of nickel loading and particle size on product distribution and coke formation, Applied Catalysis A: General, 417–418 (2012) 281-289.
[44] O.Y. Gutiérrez, T. Klimova, Effect of the support on the high activity of the (Ni)Mo/ZrO2–SBA-15 catalyst in the simultaneous hydrodesulfurization of DBT and 4,6-DMDBT, Journal of Catalysis, 281 (2011) 50-62.
[45] Y. Duan, Y. Wu, Q. Zhang, R. Ding, Y. Chen, J. Liu, M. Yang, Towards conversion of octanoic acid to liquid hydrocarbon via hydrodeoxygenation over Mo promoter nickel-based catalyst, Journal of Molecular Catalysis A: Chemical, 398 (2015) 72-78.
[46] Q. Song, F. Wang, J. Cai, Y. Wang, J. Zhang, W. Yu, J. Xu, Lignin depolymerization (LDP) in alcohol over nickel-based catalysts via a fragmentation-hydrogenolysis process, Energy & Environmental Science, 6 (2013) 994-1007.
[47] J.R. Gasson, D. Forchheim, T. Sutter, U. Hornung, A. Kruse, T. Barth, Modeling the Lignin Degradation Kinetics in an Ethanol/Formic Acid Solvolysis Approach. Part 1. Kinetic Model Development, Industrial & Engineering Chemistry Research, 51 (2012) 10595-10606.
[48] D. Forchheim, J.R. Gasson, U. Hornung, A. Kruse, T. Barth, Modeling the Lignin Degradation Kinetics in a Ethanol/Formic Acid Solvolysis Approach. Part 2. Validation and Transfer to Variable Conditions, Industrial & Engineering Chemistry Research, 51 (2012) 15053-15063.
[49] D. Forchheim, U. Hornung, A. Kruse, T. Sutter, Kinetic Modelling of Hydrothermal Lignin Depolymerisation, Waste and Biomass Valorization, 5 (2014) 985-994.
[50] A. Kloekhorst, H.J. Heeres, Catalytic Hydrotreatment of Alcell Lignin Using Supported Ru, Pd, and Cu Catalysts, ACS Sustainable Chemistry & Engineering, 3 (2015) 1905-1914.
[51] X. Huang, T.I. Korányi, M.D. Boot, E.J.M. Hensen, Catalytic Depolymerization of Lignin in Supercritical Ethanol, ChemSusChem, 7 (2014) 2276-2288.

724 [52] J. He, L. Lu, C. Zhao, D. Mei, J.A. Lercher, Mechanisms of catalytic cleavage of benzyl phenyl ether in
725 aqueous and apolar phases, Journal of Catalysis, 311 (2014) 41-51.
726 [53] T. Prasomsri, M. Shetty, K. Murugappan, Y. Roman-Leshkov, Insights into the catalytic activity and
727 surface modification of MoO3 during the hydrodeoxygenation of lignin-derived model compounds into
728 aromatic hydrocarbons under low hydrogen pressures, Energy & Environmental Science, 7 (2014) 2660-
729 2669.
730 [54] Q. Bu, H. Lei, A.H. Zacher, L. Wang, S. Ren, J. Liang, Y. Wei, Y. Liu, J. Tang, Q. Zhang, R. Ruan, A review
731 of catalytic hydrodeoxygenation of lignin-derived phenols from biomass pyrolysis, Bioresource
732 Technology, 124 (2012) 470-477.

733

734